Dispersed Phase Morphology of Impact PP Copolymers. Effects of Blend Composition as Determined by TREF

Ruth Zacur, Graciela Goizueta and Numa Capiati

Planta Piloto de Ingeniería Química - PLAPIQUI (UNS-CONICET)
Camino La Carrindanga Km 7 - (8000) Bahía Blanca - Argentina

Phone #: 54-91-4861700

Fax #: 54-91-4861600

E-mail: ncapiati@plapiqui.edu.ar

Dispersed Phase Morphology of Impact PP Copolymers. Effects of Blend Composition as Determined by TREF

Ruth Zacur, Graciela Goizueta and Numa Capiati

Planta Piloto de Ingeniería Química - PLAPIQUI (UNS-CONICET)
Camino La Carrindanga Km 7 - (8000) Bahía Blanca - Argentina

Keywords: TREF, Blend Composition, Morphology, PP Copolymers.

Polypropylene (PP) blends, commercially known as “impact polypropylene copolymers” (IPC), are produced by a sequential gas phase polymerization process. The final product is a complex mixture of polypropylene (PP) and a range of ethylene-propylene copolymers (EPC) with different ethylene contents. In the present work, the composition of three different IPC was estimated by performing a step elution mode Analytical Temperature Rising Elution Fractionation (TREF) separation. The recovered fractions were analyzed by Differential Scanning Calorimetry (DSC), Size Exclusion Chromatography (SEC) and Fourier Transform Infrared Spectroscopy (FTIR). The morphology was examined by Scanning Electron Microscopy (SEM) and Transmission Electron Microscopy (TEM). Amorphous EPC were isolated in an independent way in order to perform a more careful characterization. The distinct particle size and shape of the dispersed phase for different IPC was interpreted in terms of the molecular characteristics of the blend components and their composition.

Introduction

The IPC are heterophasic systems consisting of a complex EPC phase dispersed in a PP matrix (1-7). Consequently, it is expected that both morphology and physical properties of these materials will depend strongly on the content and molecular structure of the dispersed phase (6-7). For example, EPC containing large fractions of ethylene are crystallizable, while similar contents of ethylene and propylene yield amorphous EPC materials (1-5, 8), affecting the material morphology and properties.

The study of morphological and molecular features of complex component-composition blends requires some previous separation. The TREF technique is a well-known procedure to analyze semi-crystalline polymers through the separation of the species according to their crystallizabilities (9-10). In particular, the analytical mode of TREF was reported as an adequate technique for the quantitative analysis of polymer mixtures exhibiting dissimilar physical and chemical structures (11-14).

The elution temperature ranges of the EPC partially overlap the PP ones because the PP tacticity is always present as a distribution function (15-16). This condition precludes their complete separation along the whole elution range and the direct IPC composition evaluation. Consequently, an algebraic subtraction of the pure PP contribution to the infrared (IR) from the whole IPC signal is required (16).

In the present work three IPC materials (IPC-1, IPC-2 and IPC-3), and their corresponding major components (PP-1, PP-2 and PP-3) were fractionated by analytical TREF. A careful characterization, including SEC and DSC, of the eluted fractions was done to asses the kind of molecular species eluting at the different temperatures. Then the subtraction of the PP contribution to the IR signal, at the overlapping region with the EPC, was performed. Finally the composition was estimated. The amorphous EPC were isolated by an independent process and carefully characterized.

On the other side, the phase morphologies were analyzed by scanning electron microscopy (SEM) and transmission electron microscopy (TEM), and the composition - structure effects on the disperse phase morphology discussed.

Experimental

Materials

Commercial grade IPC samples were used in this study, which are produced industrially by a two step process: propylene is first polymerized to PP homopolymer in a stirred continuous reactor. Then it is loaded to a second reactor to be blended with a range of polymerizing EPC. For our work, samples from the second reactor (IPC-1, IPC-2 and IPC-3) were collected at the same time as their corresponding major components from the first reactor (PP-1 PP-2 and PP-3),

respectively. Pellets of the samples were produced by extrusion. Table 1 shows the average molecular weights and polydispersities for the PP homopolymers.

Fractionation by analytical TREF

Stainless steel columns (1.7 cm diameter x 25 cm length), packed with sea sand, were loaded with sample dissolved in 1,2,4, trichlorobenzene (TCB) at 140 ºC. Then, by slowly cooling the polymer solution (2 ºC/h), crystallization was achieved.

The elution procedure was performed using a stepwise temperature ramp over a temperature range of 40°C to 130 °C, by heating to the upper temperature of a desired step, holding for about 10 min, and then eluting. The effluent was monitored by IR at a fixed wavelength of 3.41 μm to detect the C-H stretching frequencies of methylene groups. The IR signals, resulting from each step, were recorded as function of the elution temperature to obtain the corresponding fractograms. Finally, the eluted samples were recovered by precipitation in cold methanol and vacuum filtration through a PTFE filter. Samples were obtained at the following final elution temperatures: 40 (only for IPC), 85, 105, 110, 115, 120 and 125 °C.

Isolation of amorphous EPC

This fractionation step was done as follows: five grams of polymer were dissolved in 250 ml of spectroscopic-grade 1,2,4-trichlorobenzene at 160°C. The solution was cooled to room temperature and kept for 24 hours. The precipitated phase was filtered and the soluble polymer

recovered by precipitation in cold methanol. This material was filtered, washed with methanol, and dried under vacuum at 40 °C.

Fractions Characterization

FTIR spectroscopy

Room temperature pressed films were used for the FTIR measurements of amorphous EPC (Nicolet 520 FTIR spectrometer, DTGS detector). The number of scans was 100 and the digital spectral resolution 4 cm^{-1} for each sample.

Differential Scanning Calorimeter (DSC)

Melting behavior and glass transition temperatures (T_g) on 10 mg samples were determined, in a Perkin Elmer DSC-7 calorimeter, under the following routine: heating from 40 ° C to 190 °C at 10°C/min, holding at 190°C for 10 min to allow the complete melting of crystallites, cooling from 190°C to 40°C at 10 °/min, holding at 40 °C during 10 min, and finally heating to 190°C, at 10 °/min, and recording the melting behavior. The temperature scale was calibrated at 10 °/min against indium (156.6 °C). Glass transition temperatures (T_g) were obtained using a heating rate of 20°/min from -140 °C to room temperature. Hexane was used as calibration standard (-95 °C).

Size Exclusion Chromatography (SEC)

Molecular weight distributions of the PP homopolymer and semi crystalline IPC fractions were determined by GPC on a Waters 150 C/V equipped with a differential refractometer detector and Millennium 2010 software. Amorphous IPC, isolated by dissolution on TCB, were simultaneously analyzed by differential refractive index and viscosity detectors. The separation was performed by three Polymer Laboratories columns (500, 10^4, 10^6 Å) using TCB at 140 °C as solvent, and a flow rate of 1.0 ml min^{-1}. The sample concentrations used for the refractive index and viscosity detection were 0.1 % and 0.25 % respectively, the injection volume 200 μl.

Phase Morphology

Press molded sheet specimens were mounted on a cryoultramicrotome LEICA UCT and microtomed to provide a new surface. The samples were microtomed at -50 ºC, then toluene etched for 1h in an ultrasonic bath, rinsed with fresh solvent to remove the dissolved polymer, and finally gold coated. SEM micrographs were obtained in a scanning electron microscope Jeol 35 CF, at a voltage of 7 kV.

Ultrathin sections of samples stained with RuO_4 vapor were cut at room temperature using a LKB ultramicrotome. TEM micrographs were obtained in a Jeol 100-CX electron microscope operated at 80 KV.

Results and Discussions

The composition calculation requires an algebraic subtraction of the pure PP infrared (IR) signal contribution from the whole IPC signal. Such subtraction can be done only when the pure PP fractionation is possible and the following conditions are fulfilled (16):

i) A non-overlapping region between PP homopolymers and the EPC exists.
ii) The presence of copolymers does not disturb the PP fractionation process.

The conditions above were verified by SEC and DSC analysis of the TREF fractions. Moreover, these results (hydrodynamic volume distributions, melting temperatures), along with comonomer contents, amorphous EPC molecular weights (measured from independently isolated amorphous fractions) and the resulting compositions were used to account for the morphological features observed by SEM and TEM.

Characterization of amorphous EPC

Figure 1 shows the thermograms obtained for the soluble fraction, after IPC dissolution in TCB and subsequent cooling to room temperature. As the three samples exhibit single glass transition temperatures (Table 2), amorphous EPC can be assumed to be their main component.

Similar compositions can be expected from EPC-1 and EPC-2 as they show equal glass transition temperatures. Furthermore, the lower T_g of EPC-3 would indicate a higher ethylene content.

Infrared spectroscopy shows the same composition tendency as T_g measurements. IR spectra are analyzed in the 1300-400 cm^{-1} wavenumber range. The ethylene content, estimated from the peak area ratios method proposed by Paroli R. M. (17) and Skaare L. E. (18) (Table 2), shows similar compositions for EPC-1 and EPC-2, and higher ethylene content for EPC-3.

Table 2 shows the average molecular weights and polydispersities for the three samples. They exhibit similar polydispersities, and the EPC-3 has the highest average molecular weights.

TREF Fractionation

Figure 2 shows the percent cumulative area under the IR signal peak, as a function of the elution temperature, for the three IPC and the corresponding PP homopolymers. It was shown before that percent area under elution peaks corresponds to percent weights (16), so we will use percent weight (% wt) instead of percent area in the following discussion.

It is clear from Figure 2 that both IPC and PP elute throughout the whole of the analyzed temperature range. For the low temperature region (up to 105°C), and due to the presence of EPC, the percent cumulative weight of the three IPC is larger than that corresponding to PP. It is also observed that the percent cumulative weight in IPC-1 is higher than in the other two

samples. Since the percent cumulative weights in all the PP fractions are similar, these results indicate that the EPC content decreases from IPC-1 to IPC-3.

Characterization of TREF fractions

Figure 3 shows the superimposed IPC and PP thermograms, corresponding to the IPC-1. For the upper temperature range (110-125°C) both the IPC fractions and the PP show a single melting peak at each temperature. The observed increase in melting peaks with the fractionation temperature indicates that the isotacticity of the fractions is also increasing. The similar melting peaks of both IPC and PP fractions, at temperatures higher than 105 °C, suggest that this sample is composed mainly by PP. Similar behavior was observed at these temperatures for IPC-2 and IPC-3.

The 105 °C thermogram for IPC-1 shows three melting peaks, while the corresponding PP fraction shows two. By comparing them, the lowest IPC-1 temperature peak (about 124°C) can be assigned, by difference, to the EPC melting. IPC-2 and IPC-3 fractions exhibited the same behavior (see Table 3).

The 85°C thermogram for IPC-1 shows one melting peak at about 108 °C (Table 3), while the corresponding PP fractions do not show any significant melting peak, indicating that these PP fractions are essentially amorphous. So, the observed peak may also be attributed to the EPC melting. Since no melting peaks were observed for the 40 °C IPC fractions, it is clear that they contain essentially amorphous material. The similar melting peaks observed for the different

IPC, eluting at the same temperature (105 and 85°C), suggest that their chemical compositions are alike (see Table 3).

Figure 4 shows the hydrodynamic volume distribution of IPC-1 fraction eluted at 40 °C and 85 °C, and PP-1 fractions from 40 °C to 85 °C. From the bimodal character of the IPC curves and by observing the overlapping region, the higher IPC volume peak can be assigned to EPC molecules, the rest being PP. Figure 5 shows the hydrodynamic volume distribution of both the IPC-1 fraction eluted at 40 °C, and the amorphous EPC previously extracted by dissolution in TCB. The absence of the lower hydrodynamic volume peak in the EPC-1 confirms the assumption made before: this sample only contains amorphous EPC. Similar results were obtained with samples IPC-2 and IPC-3.

The hydrodynamic volume distributions of the three IPC fractions, eluted at 85 °C, are shown in Figure 6. It can be observed that IPC-1 is displaced to higher hydrodynamic volumes. If we assume that the semicrystalline EPC contained in all of the IPC, have a similar chemical composition due to their similar melting temperature (about 108 °C), then the hydrodynamic volume distributions become equivalent to molecular weight distributions. So a higher molecular weight can be expected for the EPC contained in IPC-1 than for the other two.

Figure 7 shows the hydrodynamic volume distribution of the IPC-3 and PP-3 fractions eluted at 105 °C. The large hydrodynamic volume side tails are attributable to the presence of EPC molecules. Similar results were obtained in the IPC-1 and IPC-2. It was not possible to distinguish molecular weight differences between these three IPC fractions. The hydrodynamic

volume distribution obtained at temperatures higher than 105 °C for each IPC and the corresponding PP fractions did not show significant differences, suggesting that only PP is present in these IPC fractions.

Composition calculation

The results of DSC and SEC showed a reasonable evidence that no significant EPC remains above an elution temperature of 105 °C. It means that there is a region without overlapping between EPC and the PP contained in the IPC. Another observation from the experimental data is that the presence of EPC would not affect the fractionating of the PP molecules. So, the percent distribution of material (% wt), eluting at different fractionation temperatures can be calculated after the subtraction of the PP contribution to the IR signal of the IPC (16). These results are summarized in Table 4.

The total amount of EPC to be dispersed in the PP matrix is higher for the IPC-1 (22%). In all the samples the amorphous EPC are the main EPC component. IPC-3 contains the lowest ratio of amorphous EPC/total EPC (68%).

EPC distribution on the PP matrix

Figures 8a and b show the SEM micrographs of IPC-3 and IPC-2, respectively. Samples were microtomed at –50 °C and the surfaces etched in toluene before observation. Both samples show holes with sharp borders at the disperse phase particle sites. Holes may belong to

semycristalline EPC particles completely surrounded by amorphous (and toluene soluble) EPC (19). Here the particle sizes in IPC-2 are larger than in IPC-3 and the higher amount of holes observed in IPC-2 indicates a higher EPC total content in this sample.

Figure 8c shows the SEM micrograph of IPC-1. Sharp border holes are observed again. But in this case the micrograph shows also holes in which the EPC semycristalline core has remained attached to the PP after the amorphous EPC etching. These results suggest that the rubber layer, at the inclusion-matrix boundary, is interrupted by EPC semycristalline bridges. It should be pointed out that the SEM technique cannot distinguish between different crystalline phases, (for example semycristalline EPC particles embedded in a PP matrix) but reveals only the spaces occupied by rubber. If the EPC semycristalline is not completely surrounded, the rubber may appear as segregated particles of much less volume than that corresponding to the total disperse phase (20).

Figures 9a, b and c show different magnification TEM micrographs of the IPC-3 sample. It exhibits a very good RuO_4 staining for all the components, allowing the differentiation among the lamellar structures of PP, semicrystalline EPC inside the particles, and the amorphous EPC as the outer dark region of the particle. These features, and the dominant core-shell type morphology, are more clearly appreciated at high magnification (Figures 9 b and c). Moreover, from Figure 9a it is apparent that the largest particles could have been formed by the coalescence of two (or more) small particles. This effect is usual in concentrated commercial systems (21-26).

Figures 10a and b show different magnification TEM micrographs of IPC-2. Here again core-shell particle morphology is observed and the largest particles seem to be formed by coalescence like in IPC-3. The comparison of IPC-2 and IPC-3, at the same magnification (Fig. 9a and 10a), gives similar trends to the SEM results: IPC-3 contains a lower amount of disperse phase than IPC-2. Therefore, these results give an independent way to confirm the TREF composition calculation performed. On the other hand, as it was observed in the corresponding SEM micrographs (Fig. 8a and 8b), the IPC-3 particle sizes are smaller than those observed in IPC-2.

From the evidence above, it is apparent that the final disperse phase particle size is the result of a drop breakup-coalescence equilibrium. A similar mechanism was reported for industrial processes of blend mixing (21-28). Moreover, Fortenly et al. (25-26) have developed a simple equation to relate this equilibrium condition to the particle radius.

$$R = \sigma (We)_c / \eta_m \gamma + (\sigma \alpha / \eta_m f_1) \phi \qquad (1)$$

Where:

R: droplet radius

σ: interfacial tension

$(We)_c$: critical Weber number

η_m : viscosity of the matrix

γ: shear rate

α : probability of coalescence after collision

f_1 : slope of the function F (We), describing the frequency of breakups of droplets at

the critical Weber number

ϕ : the volume fraction of the disperse phase

The first term represents the droplet radius obtainable from the classical theory of break-up in an infinitely dilute dispersion. The second term determines the coalescence effect, which increases linearly with the concentration of the dispersed phase.

The particle size differences, observed in IPC-2 and IPC-3, can be qualitatively interpreted by considering the Fortenly equation. The interfacial tension (σ) between the PP matrix and the amorphous EPC depends on the ethylene content of these copolymers. However, it has been shown elsewhere (29-30) that the disperse phase particle sizes of PP/EPC blends, having similar ethylene content in EPC as in the present work (44-51%, Table 2), and equal volume fraction of dispersed phase (ϕ), are determined by the rheological parameters.

The molecular weight distributions of both PP matrix are similar (see Table 1), so their melt viscosity will be determined by the average molecular weights. The molecular weight (and consequently the viscosity) of the PP matrix, in the IPC-3 sample, is lower than in the IPC-2. Therefore, IPC-3 would exhibit lower particle break-up and higher coalescence than IPC-2 (see Eq 1).

Furthermore, the $(We)_c$ is a function of the viscosity ratio (μ) between the disperse and matrix phases ($\mu = \eta_d/\eta_m$) that reaches a minimum value when μ is about 1. The disperse phase viscosity of the IPC samples is mainly determined by their major component, the amorphous EPC (Table 4). Since the amorphous EPC in IPC-3 has almost double molecular weight than in

IPC-2 (Table 2), then the disperse phase viscosity of IPC-3 should be higher. Now, as was indicated before, the PP matrix in IPC-3 has lower viscosity than in IPC-2. So, IPC-3 has both higher disperse phase viscosity and lower matrix viscosity. In consequence, the IPC-3 samples will exhibit higher viscosity ratio (μ) and $(We)_c$ than the IPC-2.

As a result of all these effects the IPC-3 would have larger particle sizes than IPC-2, however the SEM and TEM determinations show lower particle sizes for IPC-3. As discussed, the rheological parameters of IPC-3 (disperse and matrix viscosity) would more adversely affect the final particle sizes than in IPC-2. Since the IPC-3 disperse phase content is lower than in IPC-2 (Table 4), it can be inferred that the disperse phase content predominates over the rheological properties producing stronger particle coalescence in sample IPC-2.

Figures 11a to d show different magnification micrographs of samples IPC-1. It can be observed here that EPC shows larger elongated particles than in the IPC-2 and IPC-3 samples. These particles do not show a clear phase separation between amorphous and semycristalline EPC (Figure 11b and 11c). Figure 11c shows that the semycristalline EPC is not completely surrounded by amorphous EPC. A magnified view (Figure 11d) shows this effect more clearly. This confirms the morphological features inferred by SEM: the rubber layer, at the inclusion-matrix boundary, is interrupted by EPC semycristalline bridges (Figure 8c).

The comparison of particle sizes, at the same magnification micrographs (Figures 9a, 10a and 11a), shows that IPC-1 contains the largest sizes. Here, the incidence of the dispersed phase content on the particle size is aggravated by the low molecular weight of the matrix (see Table 1),

and the higher molecular weight of the EPC components as compared with IPC-2 (see Table 2, Figure 6).

Conclusions

A careful fractionation and characterization of the main component of commercial impact copolymer was done by the TREF procedure, followed by SEC, DSC and FTIR analysis. The component contents, as calculated by the TREF analysis, shows a good qualitative agreement with the total disperse phase contents obtained by TEM. Instead the SEM results are not unambiguous when there is not complete phase separation in the dispersed phase.

A strong incidence of the dispersed phase content on droplet coalescence, and consequently on the final particle sizes, was observed. Low dispersed phase content (about 13%) tends to compensate the adverse rheological parameters effect exhibited by the studied samples. Moreover, in more concentrated systems (about 22 %) this effect is aggravated originating large and irregularly shaped domains.

- **Figure 1:** DSC thermograms of IPC soluble fractions in TCB at room temperature.
- **Figure 2:** Percent cumulative area against the elution temperature of the PP and IPC TREF fractions.
- **Figure 3:** DSC melting thermograms of IPC-1 and PP-1 TREF fractions.
- **Figure 4:** SEC hydrodynamic volume distribution of IPC-1 fraction eluted at 40 °C and 85 °C and PP-1 fractions eluted up to 85 °C.
- **Figure 5:** SEC chromatograms of IPC-1 TREF fractions eluted at 40°C and amorphous EPC-1 isolated by dissolution in TCB.
- **Figure 6:** SEC chromatograms corresponding to 85 °C fractions of IPC-1, IPC-2 and IPC-3.
- **Figure 7:** SEC chromatograms corresponding to 105 °C fractions of IPC-3 and PP-3.
- **Figure 8:** SEM micrographs of microtomed and etched: (a) IPC-3 sample, (b) IPC-2 sample and (c) IPC-1 sample
- **Figure 9:** TEM micrographs of RuO_4-stained IPC-3 sample: (a) 1cm = 1.76μm, (b) 1cm = 0.44μm and (c) 1cm = 0.11μm.
- **Figure 10:** TEM micrographs of RuO_4-stained IPC-2 sample: (a) 1cm = 1.76μm, (b) 1cm = 0.44μm.
- **Figure 11:** TEM micrographs of RuO_4-stained IPC-1 sample: (a) 1cm = 1.76μm, (b) 1cm = 1.1μm, (c) 1cm = 0.88μm and (d) 1cm = 0.11μm.

Zacur, Fig. 1

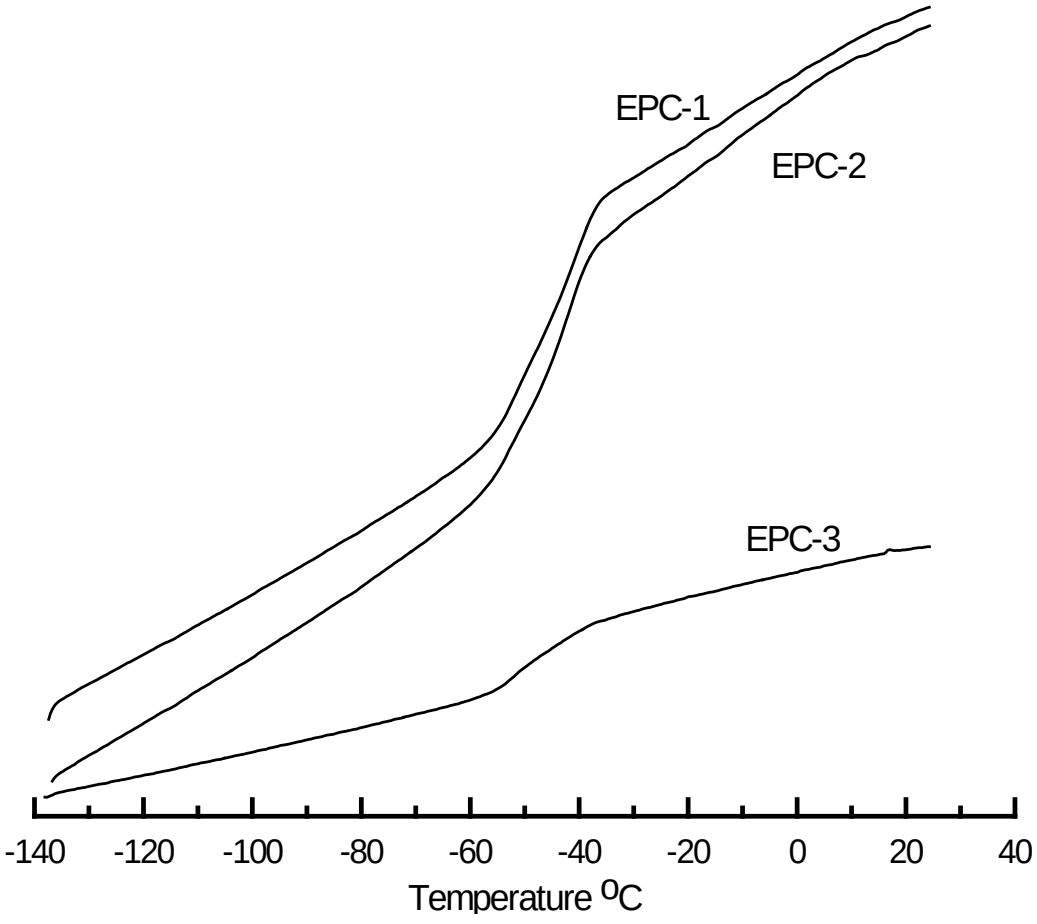

Zacur, Fig. 2

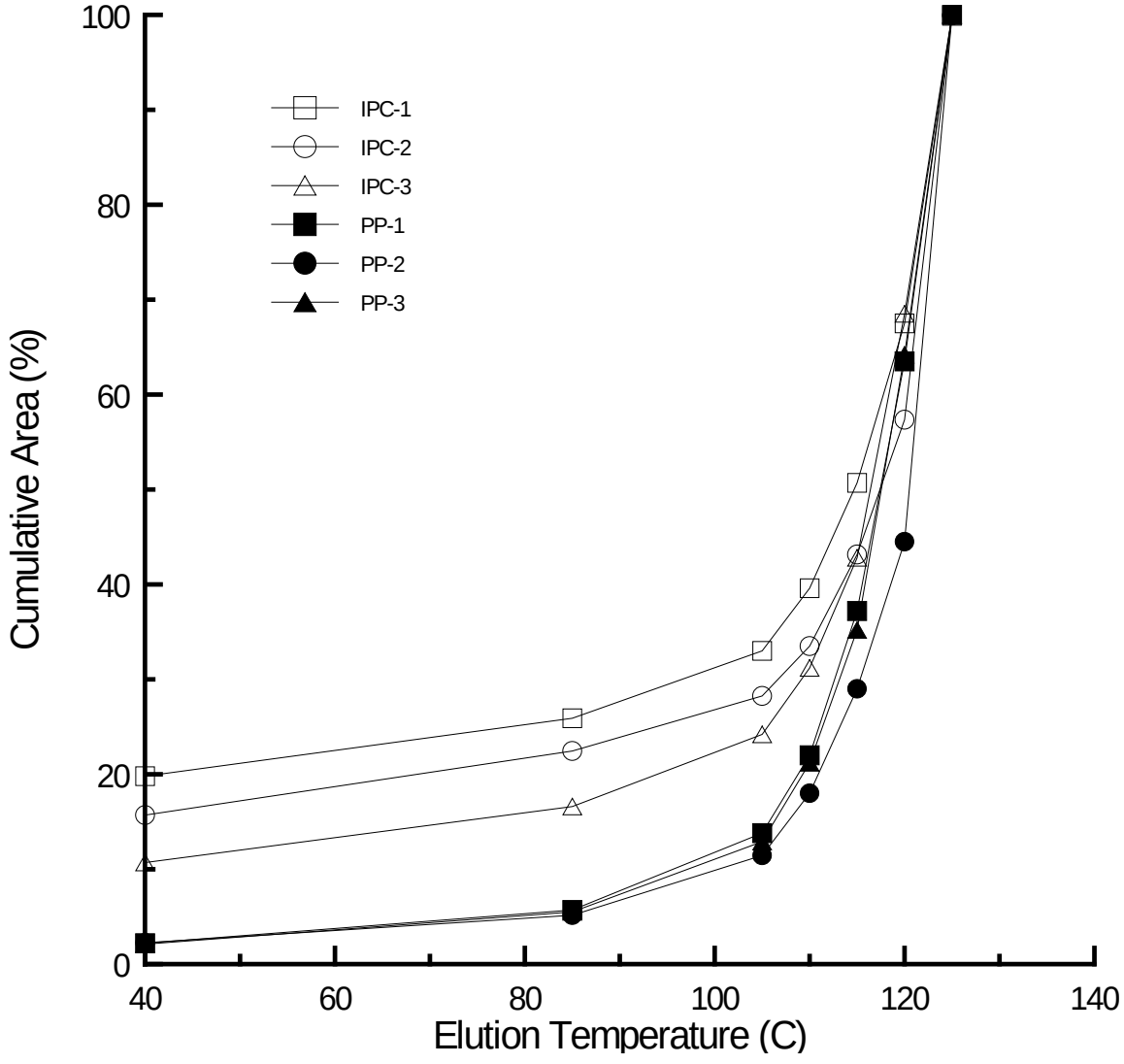
IPC-1
IPC-2
IPC-3
PP-1
PP-2
PP-3
Cumulative Area (%)
Elution Temperature (C)
0
20
40
60
80
100
40
60
80
100
120
140

Zacur, Fig.3

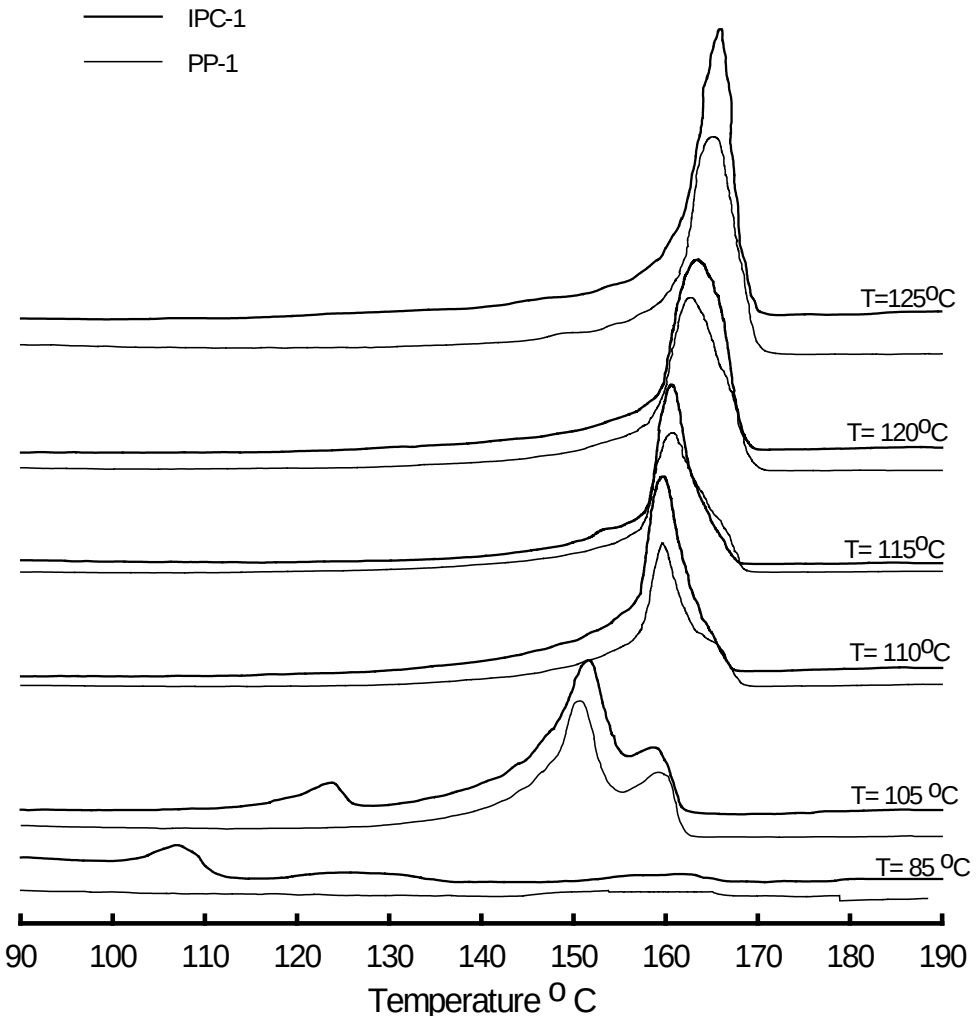
IPC-1
PP-1
T=125°C
T= 120°C
T= 115°C
T= 110°C
T= 105 °C
T= 85 °C
90
100
110
120
130
140
150
160
170
180
190
Temperature °C

Zacur, Fig. 4

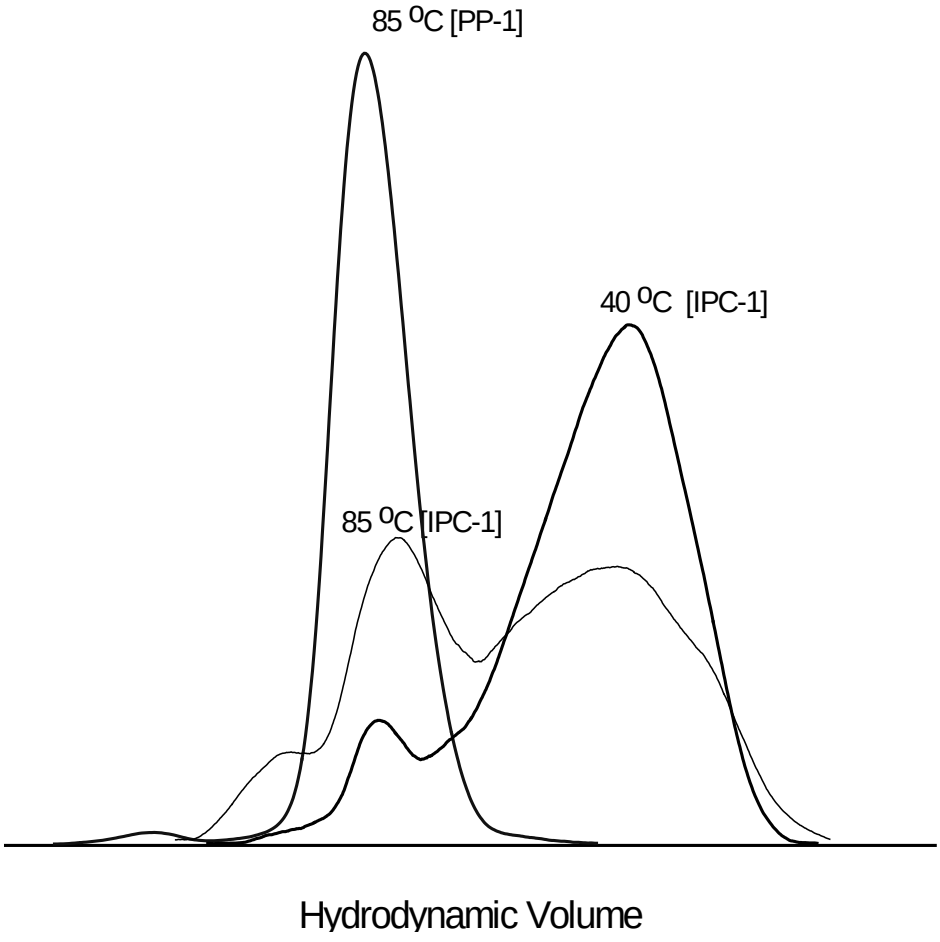

Zacur, Fig. 5

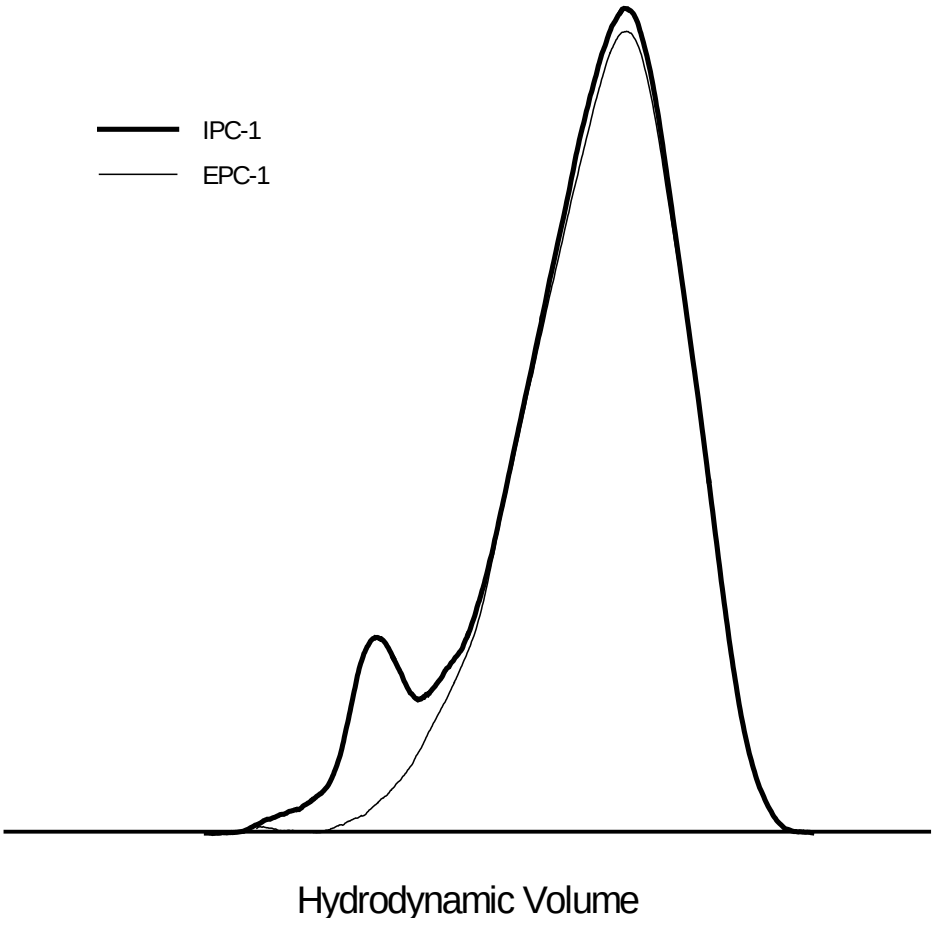

Zacur, Fig. 6

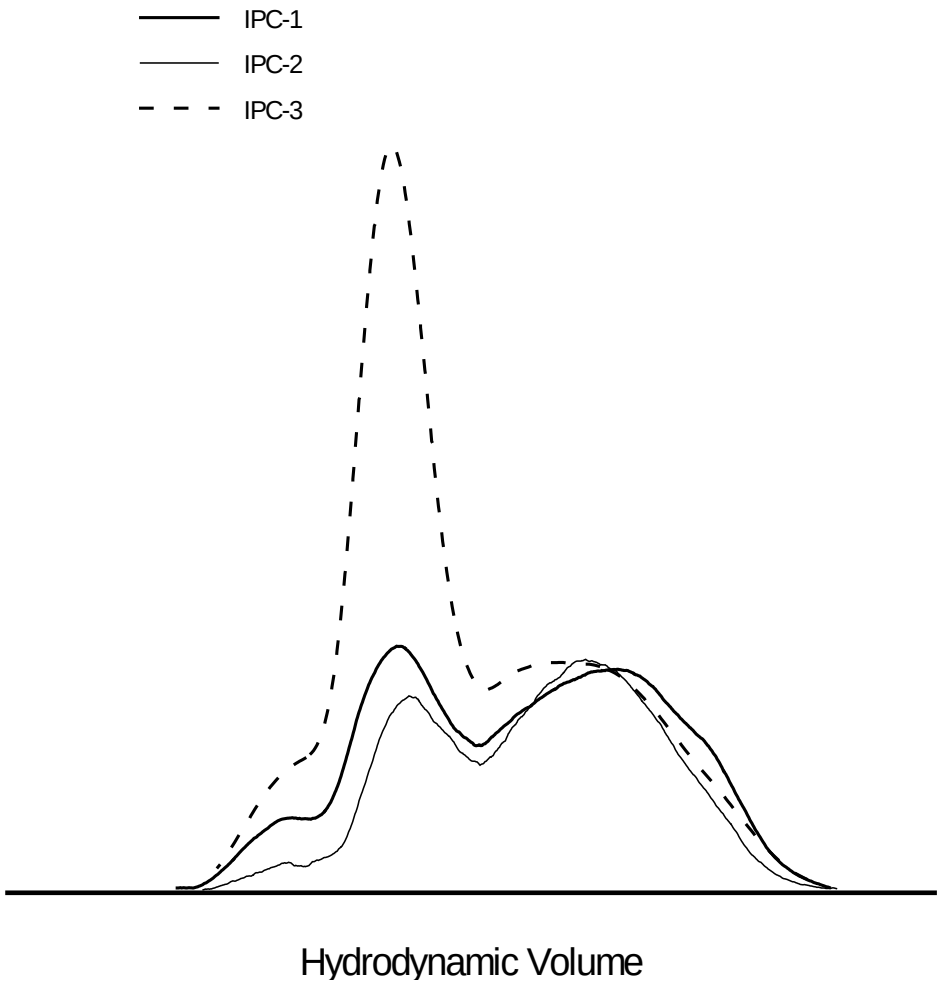

Zacur, Fig.7

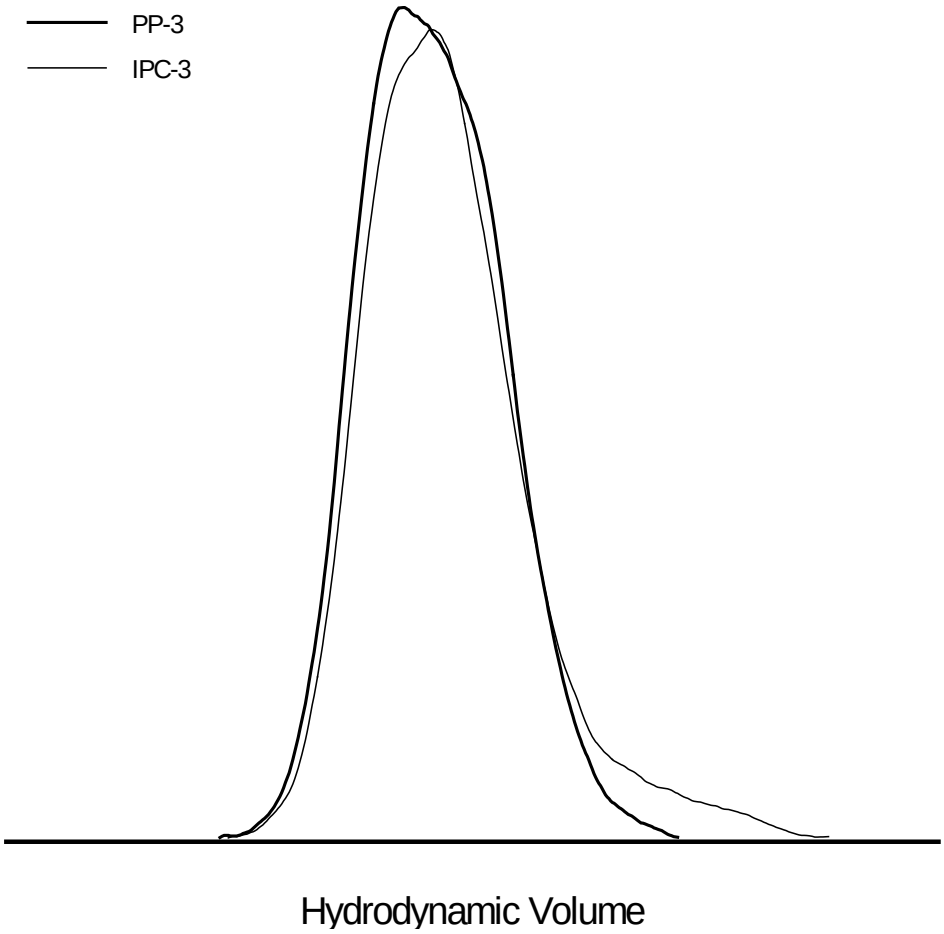

Table 1. Molecular Weight and Polydispersity of PP Materials

Sample	**M_n**	**M_w**	**M_v**	**D**
PP-1	50,000	170,000	150,000	3.4
PP-2	73,000	255,000	226,000	3.5
PP-3	42,000	160,000	140,000	3.8

Table 2. Thermal and Molecular Characterization Data for Amorphous EPC Materials

Sample	**T_g (°C)**	**Ethylene (molar %)**	**M_n**	**M_v**	**M_w**	**D**
EPC-1	- 44	45	58,000	175,000	207,000	3.6
EPC-2	- 44	44	45,000	146,000	160,000	3.5
EPC-3	- 49	51	80,000	260,000	304,000	3.8

Table 3. Thermal Characterization Data for IPC TREF Fraction

Number of fraction	Elution Temperature (°C)	IPC-1 T_m (°C)	IPC-2 T_m (°C)	IPC-3 T_m (°C)
1	40	no melting peak	no melting peak	no melting peak
2	85	108	108	109
3	105	123-151-158	123-150-159	124-150-158
4	110	158	159	158
5	115	160	160	159
6	120	163	163	163
7	125	165	164	164

Table 4. Percent Distribution of IPC Blend Components

Material	(%) PP homopolymer	(%) EPC amorphous T= 40 °C	(%) EPC crystallizable T= 85 °C	(%) EPC crystallizable T= 105 °C	Amorphous EPC / Total EPC (%)
IPC-1	78	18.2	3.4	0.6	83
IPC-2	81	13.9	4.4	0.7	73
IPC-3	87	8.9	2.9	1.2	68

References

1. E.O.Moore, Jr, *Polypropylene Handbook*, 92, Hanser Publishers, Munich (1996)
2. H. Sano, T. Usami and H. Nakagawa, *Polymer*, **27**, 1497 (1986)
3. T. Usami, Y. Gotoh, H. Umemoto and S. Takayama, *J.Appl. Polym. Sci.: Appl. Polym. Symp.*, **52**, 145 (1993)
4. T. Takahashi, H. Mizuno and E. L. Thomas, *J. Macromol. Sci.-Phys*., **B22**, 425 (1983)
5. M. Kojima, *J. Macromol. Sci., Phys. Edn*., **B19,** 523 (1981)
6. J. Karger-Kocsis, *Polypropylene Structure, Blends and Composites,*14, Chapman &Hall, London (1995)
7. E. O. Moore, Jr, *Polypropylene Handbook*, 246, Hanser Publishers, Munich (1996)
8. F. M. Mirabella Jr., *Polymer* , **34**, 1729 (1993)
9. L. Wild, T.R. Ryle, D. C. Knobeloch and I.R. Peat, *J. Polym. Sci.: Polym. Phys. Edn.*, **20**, 441 (1982)
10. F. M. Mirabella and J. F. Johnson, *J. Macromol. Sci., Rev. Macromol. Chem*., **C-12**, 81 (1975)

11. D. C. Knobeloch, and L. Wild, *SPE Polyolefins IV Conference Prepr.*, 427 (1984)

12. E. C. Kelusky, C. T. Elston and R. E. Murray, *Polym. Eng. Sci.*, **27**, 1562 (1987)

13. L. Wild, *Advances in Polymer Sci.*, **98**, 1 (1991)

14. G. Glökner, *J. Appl. Polym. Sci.:Appl. Polym. Symp.*, **45**, 1 (1990)

15. M. Kakugo, T. Miyatake, K. Mizunuma and Y. Kawai, *Macromolecules*, **21**, 2309 (1988)

16. R. Zacur , G. Goizueta and N. Capiati , *Polym. Eng. Sci*, **39**, 5, 921, (1999)

17. R. M. Paroli, J. Lara , J.J. Hhecler , K. Cole, I. Butler, *Applied Spectroscopy*, **41**, 319, (1987)

18. L.E. Skaare, P. Klaeboe, C. J. Nielsen , *Vibrational Spectroscopy*, **3,** 23, (1992)

19. F.C. Stehling, T. Huff, C. Stanley Spedd, G. Wissler, *J. Appl. Polym. Sci*, **26**, 2693, (1981)

20. N. Holz , G. Goizueta, N. Capiati , *Polym. Eng. Sci.*, **36**, 2765, (1996)

21. J.J. Elmendorp, A. K. Van der Vegt, *Polym. Eng. Sci.*, **26**, 1332, (1986)

22. P. Plochocki, S. S. Dagli, R. D. Andrews, *Polym. Eng. Sci*, , **30**, 741, (1990)

23. B. D. Favis, *J. Applied Polym Sci*., **39**, 285, (1990)

24. I. Fortelny, J. Kovar, *Eur. Polym. J.*, **25**, 317 (1989)

25. I. Fortelny, Z. Cerna, J. Binko, J. Kovar, *J. App. Polym. Sci.*, **48**, 1731, (1993)

26. I. Fortelny, A. Zivny, *Polymer*, **36**, 4113, (1995)

27. U. Sundararaj, C, W. Macosko, *Macromolecules*, **28**, 2647,(1995)

28. I. Fortelny, J. Kovar, *Polymer composites*, **9**, 119, (1988)

29. L.D'Orazio, C. Mancarella, E. Martuscelli, G. Sticotti,P. Massari, *Polymer*, **34**, 3671, (1993)

30. L.D'Orazio, C. Mancarella, E. Martuscelli, F. Polato, *Polymer*, **32**, 1186, (1991)